Emergence of classicality under decoherence in near steady-state robust quantum transport

S. Schirmer, *Member, IEEE,* E. Jonckheere, *Life Fellow, IEEE*, S. O'Neil, and F. Langbein, *Member, IEEE*

***Abstract*—In the quantum analogue of the classical feedback problem of driving the state to a desired terminal target, several highly nonclassical features emerge—in particular, the lack of closed-loop stability in case of purely coherent dynamics where Schrödinger equation prevails and a challenge to the classical limitation of conflict between precision of targeting and sensitivity of targeting error to parameter uncertainty. Here we show that given a quantum system evolving according to a fixed Hamiltonian and pure dephasing we recover classicality, in the sense that the closed-loop system is stable and that the classical limitations re-emerge.**

I. Introduction

Recently, a new paradigm for quantum control based on energy landscape shaping has been proposed and applied to derive feedback control laws for selective transfer of excitations between nodes of a network consisting of N coupled spins [1]. The controllers $D(|\mathrm{IN}\rangle, |\mathrm{OUT}\rangle)$ are designed to maximize the fidelity $F := |\langle \mathrm{OUT}| U(t_f) |\mathrm{IN}\rangle|$ of transfer from the input quantum state $|\mathrm{IN}\rangle$ to the output state $|\mathrm{OUT}\rangle$ at a specified readout time t_f, where $U(t)$ is the unitary time-evolution operator of the system, relying only on static bias fields $\{D_n\}_{n=1}^N$ applied to their respective spins to shift the energy levels of the system [2], obviating the need for, and side-stepping the back-action of, measurements.

The presumption that the bias fields are spin-addressable calls into question the issue of robustness of the design. Even though current technological advances are targeting such objective [3], field focusing errors are always going to be present to some extent. Next to this *bias spillage* issue, uncertainties in the (possibly engineered) spin couplings are also present. Differential sensitivity analyses against such uncertainties have led to the surprising result that controllers with the best fidelity yields a design with performance least sensitive to coupling errors—a feature that goes against conventional control wisdom [4].

This classical-quantum discrepancy is not surprising given that the optimal controllers described above are selective, that is, no input other than $|\mathrm{IN}\rangle$ can drive the system to $|\mathrm{OUT}\rangle$. Furthermore, unlike classical robust control, the target states are not asymptotically stable but rather the system is oscillating around the target state, similar to the case of Anderson localization [5], although localization is achieved through control biases and no randomness is required.

The aforementioned uncertainties, while they apply to non-classical quantum systems, are still classical in the sense that they model parameter uncertainties in the plant and in the controller, to borrow classical phraseology. In addition to classical uncertainties, quantum systems exhibit uncertainties that do not fit within the classical robustness paradigm: namely, preparation errors in the initial state $|\mathrm{IN}\rangle$ and, last but not least, uncertainties in the decoherence process. Ref. [3] specifically addresses the large, structured properties of the uncertainties using the μ-function [6] and only tacitly introduces initial state preparation error as extraneous perturbation. Ref [7] focuses on the effect of uncertainties lumped in the decoherence process, disregarding all other uncertainties.

In the present paper, which follows in the footsteps of [8], we consider another mix. We consider coupling errors, bias spillage, and initial preparation error, under a fixed Lindblad decoherence process, where the rates have been randomly drawn to avoid biases. The primary objective of this somewhat preliminary study is to expose a shift from anticlassical to classical robustness properties as a result of the decoherence. To be somewhat more specific, we look at how the transmission T from the initial state preparation error to the error $\varepsilon := 1 - F^2$ is affected by large perturbation in the couplings and bias fields. Those uncertainties are embedded in T as an upper linear fractional transformation $\mathcal{F}_u(G, \Delta)$ of the diagonal model Δ of the uncertainty under a 2×2 coupling matrix G, as shown by Fig. 1. The sensitivity of T to large variation is quantified using $\mu(G)$. We consider a variety of controllers achieving a variety of F's and $\mu(G)$'s and examine discordance or concordance between F and $\mu(G)$ using statistical techniques. Discordance, that is, F increases (decreases) while $\mu(G)$ decreases (increases) across some ordering of the controllers is anticlassical and manifests itself for coherent systems, whereas under decoherence the trend shifts to classical concordance, that is, F and $\mu(G)$ either simultaneously increases or decrease across a family of ordered controllers.

This anticlassical to classical transition under decoherence is consistent with some arguments that decoherence may provide the quantum-to-classical bridge that makes the macro world classical (e.g., [9], [10] and references therein), although some of these arguments are controversial.

II. Spin networks under Decoherence

In this section we briefly review the theory of quantum spin networks subject decoherence and derive the relevant single

S. Schirmer is with Swansea University, Swansea, UK, lw1660@gmail.com.

E. Jonckheere is with the University of Southern California, Los Angeles, CA, jonckhee@usc.edu.

S. O'Neil is with US Military Academy, West Point, NY, sean.o'neil@westpoimnt.edu.

F. Langbein is with Cardiff University, Cardiff, UK, LangbeinFC@cardiff.ac.uk.

excitation subspace dynamics.

A. Lindblad equation for spin networks

Our starting point is a network of N interacting spin-$\frac{1}{2}$ particles arranged in a ring structure with near neighbor couplings and bias fields specified by the $2^N \times 2^N$ total Hamiltonian

$$\mathbf{H_D} = \underbrace{\sum_{n=1}^{N} J_{n,n+1}(\mathbf{X}_n\mathbf{X}_{n+1} + \mathbf{Y}_n\mathbf{Y}_{n+1} + \kappa\mathbf{Z}_n\mathbf{Z}_{n+1}) + h.c.}_{\mathbf{H}} + \underbrace{\sum_{n=1}^{N} D_n\mathbf{Z}_n}_{\mathbf{D}}. \quad (1)$$

In the above, $\mathbf{X}_n$, $\mathbf{Y}_n$, $\mathbf{Z}_n$ are the Pauli spin operators acting on spin n. These are N-fold tensor products whose nth factor is one of the Pauli matrices

$$X = \begin{pmatrix} 0 & 1 \\ 1 & 0 \end{pmatrix}, \quad Y = \begin{pmatrix} 0 & -\jmath \\ \jmath & 0 \end{pmatrix}, \quad Z = \begin{pmatrix} 1 & 0 \\ 0 & -1 \end{pmatrix},$$

and all other factors are the 2×2 identity matrix I. The parameter κ is used to distinguish XX-coupling ($\kappa = 0$) from Heisenberg coupling ($\kappa = 1$). $J_{n,n+1}$ denotes the strength of the coupling between spins n and $n+1$, with the understanding that $J_{N,N+1} = J_{N,1}$ to enforce the ring structure. D_n is the static bias field addressing spin n.

The state of the system at time t can be described by a $2^N \times 2^N$ density operator $\varrho(t)$. If the system is weakly coupled to an environment, then the evolution is governed by the Lindblad equation

$$\dot{\varrho}(t) = -\jmath[\mathbf{H_D}, \varrho(t)] + \mathbf{L_D}(\varrho(t)), \quad (2)$$

where $\mathbf{H_D}$ is the Hamiltonian defined above and $\mathbf{L_D}$ is a Lindblad super-operator

$$\mathbf{L_D}(\varrho) = \mathbf{V_D}\varrho\mathbf{V_D} - \tfrac{1}{2}(\mathbf{V_D}^\dagger\mathbf{V_D}\varrho + \varrho\mathbf{V_D}^\dagger\mathbf{V_D}). \quad (3)$$

Setting $\mathbf{V_D} = 0$ we recover the usual Hamiltonian dynamics considered in previous work [1]. In this paper we are mostly interested in systems subject to decoherence that can be modelled as dephasing in the Hamiltonian basis. This is a common model for weak decoherence and can be described by a Lindblad operator $\mathbf{L_D}$ of dephasing type, given by a Hermitian dephasing operator that commutes with the system Hamiltonian,

$$\mathbf{V_D} = \mathbf{V_D}^\dagger, \quad [\mathbf{H_D}, \mathbf{V_D}] = 0. \quad (4)$$

The subscript $\mathbf{D}$ in the Lindbladian indicates a dependence on the control; indeed, strictly speaking, decoherence in the weak coupling limit depends on the total Hamiltonian and hence on the control [11], [12]. Although this is a very simple decoherence model, it is easily seen that this model is closer to the master equation in the weak coupling limit developed in [12] than it appears at a first glance. For $\mathbf{V_D}$ Hermitian, it can easily be verified that the Lindblad superoperator can be simplified

$$\mathbf{L_D}(\varrho) = -\tfrac{1}{2}[\mathbf{V_D}, [\mathbf{V_D}, \varrho]]. \quad (5)$$

As $\mathbf{H_D}$ and $\mathbf{V_D}$ commute, they are simultaneously diagonalizable and there exists a set of projectors $\{\Pi_k(\mathbf{H_D})\}_k$ onto the (orthogonal) simultaneous eigenspaces of $\mathbf{H_D}$ and $\mathbf{V_D}$ such that $\sum_k \Pi_k(\mathbf{H_D}) = \mathbf{I}_{C^{2^N}}$ is a resolution of the identity on the full Hilbert space $\mathbb{C}^{2^N}$ and

$$\mathbf{H_D} = \sum_k \lambda_k(\mathbf{H_D})\Pi_k(\mathbf{H_D}), \quad \mathbf{V_D} = \sum_k \mathbf{c}_k\Pi_k(\mathbf{H_D}),$$

where $\lambda_k(\mathbf{H_D})$ and $\mathbf{c}_k$ are the respective real eigenvalues of $\mathbf{H_D}$ and $\mathbf{V_D}$.

Pre-/post-multiplying the master equation (2) with Lindblad term (5) by $\Pi_k(\mathbf{H_D})$ and $\Pi_\ell(\mathbf{H_D})$, respectively, yields

$$\Pi_k(\mathbf{H_D})\dot{\varrho}(t)\Pi_\ell(\mathbf{H_D}) = (-\jmath\omega_{k\ell} + \gamma_{k\ell})\Pi_k(\mathbf{H_D})\varrho(t)\Pi_\ell(\mathbf{H_D}), \quad (6)$$

with $\boldsymbol{\omega}_{k\ell} = \lambda_k(\mathbf{H_D}) - \lambda_\ell(\mathbf{H_D})$ and $\boldsymbol{\gamma}_{k\ell} = -\frac{1}{2}(\mathbf{c}_k - \mathbf{c}_\ell)^2 \leq 0$. The solution to this equation is

$$\Pi_k(\mathbf{H_D})\varrho(t)\Pi_\ell(\mathbf{H_D}) = e^{-t(\jmath\boldsymbol{\omega}_{k\ell} - \boldsymbol{\gamma}_{k\ell})}\Pi_k(\mathbf{H_D})\varrho_0\Pi_\ell(\mathbf{H_D}).$$

The above clearly shows the decoherence $\boldsymbol{\gamma}_{k\ell}$ acting on the subspace $\Pi_k(\mathbf{H_D})\varrho\Pi_\ell(\mathbf{H_D})$. Since $\sum_k \Pi_k(\mathbf{H_D}) = \mathbf{I}$, the full solution is found as $\varrho(t) = \sum_{k,\ell} \Pi_k(\mathbf{H_D})\varrho(t)\Pi_\ell(\mathbf{H_D})$, which yields

$$\varrho(t) = \sum_{k,\ell} e^{-t(\jmath\boldsymbol{\omega}_{k\ell} - \boldsymbol{\gamma}_{k\ell})}\Pi_k(\mathbf{H_D})\varrho_0\Pi_\ell(\mathbf{H_D}). \quad (7)$$

B. Reduced (single excitation subspace) model

It is easily seen that the total spin operator

$$\mathbf{S} = \frac{1}{2}\sum_{n=1}^{N}(\mathbf{I} + \mathbf{Z}_n) \quad (8)$$

counts the number of spins up (excited spins). Furthermore, it is not too hard to verify that $[\mathbf{H_D}, \mathbf{S}] = 0$, $\forall D_n$. Therefore, $\mathbf{H_D}$ and $\mathbf{S}$ have the same eigenspaces. We will in particular retain the eigenspace of $\mathbf{S}$ corresponding to the eigenvalue 1, and refer to it as the *single excitation subspace*. Since it is also an eigenspace of $\mathbf{H_D}$, it is invariant under the Hamiltonian dynamics.

Since $[\mathbf{H_D}, \mathbf{S}] = 0$, the single excitation subspace is made up of eigenspaces of $\mathbf{H_D}$. Let $\mathcal{K}$ be the set of indexes of the eigenspaces of $\mathbf{H_D}$ that span the single excitation subspace, i.e., the eigenspace of $\mathbf{S}$ with eigenvalue 1, and define the single-excitation subspace operators

$$V_D = \sum_{k\in\mathcal{K}} c_k\Pi_k(\mathbf{H_D}), \quad (9a)$$

$$H_D = \sum_{k\in\mathcal{K}} \lambda_k\Pi_k(\mathbf{H_D}), \quad (9b)$$

$$\rho = \sum_{k,\ell\in\mathcal{K}} \Pi_k(\mathbf{H_D})\varrho\Pi_\ell(\mathbf{H_D}). \quad (9c)$$

Then the reduced Lindblad-Liouville equation is

$$\dot{\rho} = -\jmath[H_D, \rho] + V_D\rho V_D - \tfrac{1}{2}(V_D^2\rho + \rho V_D^2) \quad (10)$$

and Eq. (7) shows that the solution is

$$\rho(t) = \sum_{k,\ell \in \mathcal{K}} e^{-t(\jmath\omega_{k\ell} - \gamma_{k,\ell})} \Pi_k(H_D) \rho_0 \Pi_\ell(H_D), \qquad (11)$$

where

$$\omega_{k\ell} = \lambda_k(H_D) - \lambda_\ell(H_D), \quad \gamma_{k,\ell} = -\tfrac{1}{2}(c_k - c_\ell)^2. \qquad (12)$$

In the single excitation formulas, $\mathcal{K}$ will denote the set of indices of *distinct* eigenvalues.

Given the ring structure, this procedure yields the single excitation subspace Hamiltonian of the controlled system

$$H_D = \begin{pmatrix} D_1 & J_{12} & 0 & \dots & 0 & J_{N,1} \\ J_{12} & D_2 & J_{23} & & 0 & 0 \\ 0 & J_{23} & D_3 & & 0 & 0 \\ \vdots & & \ddots & \ddots & \ddots & \vdots \\ 0 & 0 & 0 & & D_{N-1} & J_{N-1,N} \\ J_{N,1} & 0 & 0 & \dots & J_{N-1,N} & D_N \end{pmatrix}. \qquad (13)$$

Perturbations of the $J_{n,n+1}$'s and $J_{N,1}$ do not change the structure of $\mathbf{H_D}$ and hence do not affect the commutativity relation between $\mathbf{H_D}$ and $\mathbf{S}$. Similarly, errors in the field focusing only affect the D_n's and hence do not affect the structure of $\mathbf{H_D}$. Therefore, invariance of the single excitation subspace is maintained under both near-neighbor coupling strength and bias control field perturbations.

Note that Sec. II-A remains valid when $\mathbf{V} = \mathbf{S}$. In this case of collective dephasing, $\boldsymbol{c}_k$ are the eigenvalues of $\mathbf{S}$, $c_k = 1$ on the single excitation subspace, and the single excitation subspace is a decoherence free subspace [13, Sec. III.B].

C. Steady-state versus Long-term average

As already noted, the coherent movement lacks asymptotic stability; therefore, $\lim_{t\to\infty}$ cannot be dealt with using the classical Laplace final value theorem. However, the following comes to the rescue:

Lemma 1: Nonclassical Laplace final value [14, Th. 2]. Let $\hat{f}(s)$ be the Laplace transform of $f(t)$. If

$$\lim_{s\to 0} \int_s^\infty \frac{\hat{f}(\xi)}{\xi} d\xi = \infty,$$

then

$$\lim_{t_f\to\infty} \frac{1}{t_f} \int_0^{t_f} f(t)dt = \lim_{s\to 0} s\hat{f}(s).$$

■

Using this lemma and (11) the following is easily proved:

Theorem 1: For the coherent motion, the *long term average* is

$$\lim_{T\to\infty} \frac{1}{T} \int_0^T \rho(t)dt = \lim_{s\to 0} s\hat{\rho}(s) \qquad (14)$$

$$= \sum_k \Pi_k(H_D) \rho_0 \Pi_k(H_D), \qquad (15)$$

whereas for the decoherent motion the *steady-state* solution is

$$\rho_\infty := \lim_{t\to\infty} \rho(t) = \sum_k \Pi_k(H_D) \rho_0 \Pi_k(H_D).$$

Proof. For the coherent motion, set $c_k = 0$, which yields $\gamma_{k\ell} = 0$ in (11). The poles of $\hat{\rho}(s)$ are $\jmath\omega_{k\ell}$. By the generalized Laplace final value theorem, the long-term average is the residue of $\hat{\rho}(s)$ at $s = 0$. The pole at $s = 0$ is obtained by setting $k = \ell$ in (11) and the result follows. Regarding the decoherent motion, observe that all terms $k \neq \ell$ in (11) vanish as $t \to \infty$, so that only the $k = \ell$ terms are involved in the steady-state and the result follows. ■

It is important to note that the decoherence is lost under steady-state, so that the effect of decoherence cannot be gauged from a strict steady-state situation. This is the reason why the transmission $T(s)$ will be evaluated at $s = \epsilon > 0$, not 0, as argued in Sec. IV-B.

III. Computations—Bloch equation formulation

To facilitate the following analysis we reformulate the Lindblad equation (10) in the standard state-space format by expanding with respect to a basis $\mathcal{B} = \{\sigma_i\}_{i=1}^{N^2}$ for the $N \times N$ Hermitian operators. If $\mathcal{B}$ is orthonormal, i.e., $\mathrm{Tr}(\sigma_i\sigma_j) = \delta_{ij}$, then the master equation (10) can be written in coordinate form as a linear matrix differential equation for the state vector $\boldsymbol{r} = (r_1, ..., r_{N^2})^T \in \mathbb{R}^{N^2}$ with $r_i = \mathrm{Tr}(\rho\sigma_i)$. Defining A_D to be the $N^2 \times N^2$ real matrix

$$(A_D)_{ij} = \mathtt{H}_{k\ell} + \mathtt{D}_{ij} + \mathtt{L}_{ij}, \quad 1 \le i, j \le N^2, \qquad (16)$$

where $\mathtt{H}$, $\mathtt{D}$ and $\mathtt{L}$ are $N^2 \times N^2$ (real) matrices with entries [15, Eq. (4)]

$$\mathtt{H}_{ij} = \mathrm{Tr}(\jmath H[\sigma_i, \sigma_j]), \qquad (17a)$$

$$\mathtt{D}_{ij} = \mathrm{Tr}(\jmath D[\sigma_i, \sigma_j]), \qquad (17b)$$

$$\mathtt{L}_{ij} = \mathrm{Tr}(V_D\sigma_i V\sigma_j) - \tfrac{1}{2}\mathrm{Tr}(V_D^2\{\sigma_i, \sigma_j\}), \qquad (17c)$$

where $\{A, B\} = AB + BA$ is the usual anticommutator and V_D is the decoherence operator from Eq. (10), the linear matrix differential equation for $\boldsymbol{r}$ becomes

$$\dot{\boldsymbol{r}}(t) = A_D\boldsymbol{r}(t). \qquad (18)$$

The $N^2 \times N^2$ matrix A_D constructed from (17) is singular with at least N zero eigenvalues. This can easily be seen by pre- and postmultiplying (11) by $\Pi_{k\in\mathcal{K}}$, which yields $\Pi_k\rho(t)\Pi_k = \Pi_k\rho(0)\Pi_k$, and shows that $\rho(t)$ is constant along at least N directions.

In the single excitation subspace a convenient standard basis is given by the generalized Pauli or Gell-Mann basis [16] of $N \times N$ trace-zero Hermitian matrices

$$x_{ij} := (1/\sqrt{2})(E_{ij} + E_{ji}) : 1 \le i < j \le N,$$
$$y_{ij} := (-\jmath/\sqrt{2})(E_{ij} - E_{ji}) : 1 \le i < j \le N,$$
$$z_i := (1/\sqrt{i+i^2})\left(I_{i\times i} \oplus \{-i\} \oplus 0_{(N-i-1)\times(N-i-1)}\right) : 1 \le i \le N-1,$$

where E_{ij} be the matrix with zeros everywhere except for 1 in entry (i, j). Let $\{\sigma_i\}_{i=1}^{N(N-1)}$ be the basis elements with off-diagonal terms and $\{\sigma_i\}_{i=N^2-N+1}^{N^2-1}$ be the $N-1$ diagonal, trace-zero basis elements. This basis for the trace-zero Hermitian matrices and be extended to a basis for *all* Hermitian matrices by adding $\sigma_{N^2} := (1/\sqrt{N})I_{N\times N}$. If we

specialize the Bloch equations to the Gell-Mann basis, it is easily seen that

$$\begin{aligned} &\mathtt{H}_{i,N}=0, \qquad &&\mathtt{D}_{i,N}=0, \quad &&\mathtt{L}_{i,N}=0, \qquad &&\forall i,\\ &\mathtt{H}_{N,j}=0, \qquad &&\mathtt{D}_{N,j}=0, \quad &&\mathtt{L}_{N,j}=0, \qquad &&\forall j, \end{aligned}$$

i.e., the last row and column of A_D vanish and A_D has an eigenvalue at 0, among those already observed. Note that since $\sigma_{N^2} = \frac{1}{\sqrt{N}} I_{N\times N}$ it is easily seen that $r_{N^2}(t) = \frac{1}{\sqrt{N}}\operatorname{Tr}(\rho(t)) = \frac{1}{\sqrt{N}}$ and thus $\dot{r}_{N^2}(t) = 0$, consistent with the fact that r_{N^2} denotes the (normalized) trace of the density, which must remain constant. We can define the so-called reduced Bloch vector

$$\boldsymbol{s} = (r_1, \ldots, r_{N^2-1})^T,$$

and rewrite the Lindblad equation for $\boldsymbol{r}$ as

$$\dot{\boldsymbol{s}}(t) = \bar{A}_D \boldsymbol{s}(t), \tag{19}$$

where $\bar{A}_D$ is the $(N^2-1)\times(N^2-1)$ submatrix of A_D obtained by deleting the final row and column of A_D.

IV. Control Objectives

A. State space error signal

The primary control objective is to steer the dynamics to maximize the transfer fidelity $F(t)$ from a local excitation state $|\mathrm{IN}\rangle$ at an input node of the spin network to another state of excitation $|\mathrm{OUT}\rangle$ at the output node, or equivalently to maximize the probability p_t of successful transfer

$$F^2(t) = p_t(|\mathrm{IN}\rangle \to |\mathrm{OUT}\rangle) = \langle \mathrm{OUT}|\, \rho(t)\, |\mathrm{OUT}\rangle\,. \tag{20}$$

Depending on the application, we could consider either the instantaneous transfer fidelity at certain time t, or a steady-state asymptotic fidelity as $t \to \infty$, or even a time-averaged fidelity. For the time being, we consider a generic error

$$\varepsilon_t = 1 - \langle \mathrm{OUT}|\rho(t)|\mathrm{OUT}\rangle$$

and note that it can be rewritten as

$$\varepsilon_t = \operatorname{Trace}\left((I - |\mathrm{OUT}\rangle\langle\mathrm{OUT}|)\rho(t)\right).$$

Define $P_{\mathrm{OUT}} = |\mathrm{OUT}\rangle\langle\mathrm{OUT}|$ to be the orthogonal projection on the $|\mathrm{OUT}\rangle$ subspace and $P_{\mathrm{OUT}^\perp} = I - |\mathrm{OUT}\rangle\langle\mathrm{OUT}|$ the projection on $\mathrm{OUT}^\perp$. Let $\{f_n\}_{n=1}^{N-1}$ be an orthonormal basis of the orthogonal complement $|\mathrm{OUT}\rangle^\perp$ of the target state. Then using $I - |\mathrm{OUT}\rangle\langle\mathrm{OUT}| = \sum_n |f_n\rangle\langle f_n|$, the error can be rewritten as

$$\varepsilon_t = \sum_n \langle f_n|\rho(t)|f_n\rangle.$$

The above appears to be the natural choice for an error signal $z(t)$ that has to be kept "small" in a robust design. However, for reasons related to the justification of the "fictitious feedback" of such design, we prefer to redefine the error output as

$$z(t) = \begin{pmatrix} \langle f_1|\rho(t)|f_1\rangle \\ \vdots \\ \langle f_{N-1}|\rho(t)|f_{N-1}\rangle \end{pmatrix}.$$

(See Appendix C.)

Expanding ρ with respect to the basis $\{\sigma_k\}_{k=1}^{N^2}$ of the set of Hermitian operators chosen in Sec. III, $\rho = \sum_k r_k\sigma_k$, then yields

$$z(t) = \sum_{k=1}^{N^2} \begin{pmatrix} \langle f_1|\sigma_k|f_1\rangle \\ \vdots \\ \langle f_{N-1}|\sigma_k|f_{N-1}\rangle \end{pmatrix} r_k(t). \tag{21}$$

Therefore, the output variable can be written as $z(t) = C\boldsymbol{r}(t)$ where

$$C = \begin{pmatrix} \langle f_1|\,\sigma_1\,|f_1\rangle & \ldots & \langle f_1|\,\sigma_{N^2}\,|f_1\rangle \\ \vdots & & \vdots \\ \langle f_{N-1}|\,\sigma_1\,|f_{N-1}\rangle & \ldots & \langle f_{N-1}|\,\sigma_{N^2}\,|f_{N-1}\rangle \end{pmatrix}. \tag{22}$$

These equations are redundant as we did not enforce the trace 1 property of ρ, but we will take care of this in the following section.

If $|\mathrm{IN}\rangle$ is a natural basis vector, as it happens when $|\mathrm{IN}\rangle$ is an excitation localized at one spin, the f_n's in Eq. (22) can be chosen as natural basis vectors as well, so that the first $N^2 - N$ columns of C vanish. It is also easily observed that the last column of C is $(1/\sqrt{N})\mathbf{1}_{N-1}$, where $\mathbf{1}_{N-1}$ denotes the $(N-1)$-dimensional column vector made up of 1's. Thus the output matrix takes the form

$$C = \left(0_{(N-1)\times(N^2-N)}\,|\,\{\langle f_n|\sigma_k|f_n\rangle\}\,|\,\tfrac{1}{\sqrt{N}}\mathbf{1}_{N-1}\right), \tag{23}$$

where $n = 1, \ldots, N-1$ and $k = N^2 - N + 1, \ldots, N^2 - 1$, and taking $\bar{C}$ to be the reduced C-matrix comprised of its first $N^2 - 1$ columns

$$\boldsymbol{z} = C\boldsymbol{r} = \bar{C}\boldsymbol{s} + \tfrac{1}{N}\mathbf{1}_{N-1}. \tag{24}$$

B. Intermediate, near stead-state, regime

Having defined the error signal $z(t)$, we now refine the definition of the transmission T introduced in the introduction. We define $T(s)$ to be the transmission from an initial state preparation error to $\hat{z}(s)$, but this leaves the question of where to evaluate $T(s)$ in $\Re s > 0$. Referring to Sec. II-C, taking $s = 0$ would wipe out the decoherence, although sensitivity to coupling and bias field errors can still be evaluated through H_D. We opt for an intermediate regime $s = \epsilon > 0$ noting that

$$\hat{z}(\epsilon) = \int_0^\infty e^{-\epsilon t} z(t) dt. \tag{25}$$

Heuristically, as argued in [3], this could be justified on the ground that once the process is initiated the initial state preparation error remains constant. It could as well be justified by the $1/f$ noise in SQUID qubits [17].

V. Sensitivity of asymptotic transfer probability

When the transfer time is long compared to the time required for the system to reach a steady state, it is useful to consider the sensitivity of the asymptotic probability of transfer (squared fidelity) $p_\infty = \langle \mathrm{OUT}|\,\rho_\infty\,|\mathrm{OUT}\rangle$ and compute the log-sensitivity in the same manner as [4]. Using the perturbed, controlled Hamiltonian $\widetilde{H}_D = H_D + \delta S_{H_D}$, where

S_{H_D} indicates the structure of the perturbation and δ its size, we have from (20) and Th. 1,

$$p_\infty = \sum_{k=1}^{N} \langle \mathrm{OUT}| \, \Pi_k(\widetilde{H}_D)\rho_0\Pi_k(\widetilde{H}_D) \, |\mathrm{OUT}\rangle$$

with $\rho_0 = |\mathrm{IN}\rangle \langle \mathrm{IN}|$. Note that with the upper limit of the sum to be N it is assumed that the perturbation is a *universal unfolding* [18] of the multiple eigenvalue singularity, that is, the perturbation splits all multiple eigenvalues into simple ones. Under this assumption, the derivative

$$\begin{aligned}\frac{\partial p_\infty}{\partial \delta} =& \sum_{k=1}^{N} \langle \mathrm{OUT}| \, \frac{\partial \Pi_k(\widetilde{H}_D)}{\partial \delta}\rho_0\Pi_k(\widetilde{H}_D) \, |\mathrm{OUT}\rangle \\ &+ \sum_{k=1}^{N} \langle \mathrm{OUT}| \, \Pi_k(\widetilde{H}_D)\rho_0 \frac{\partial \Pi_k(\widetilde{H}_D)}{\partial \delta} \, |\mathrm{OUT}\rangle \\ =& 2\Re \sum_{k=1}^{N} \langle \mathrm{OUT}| \, \frac{\partial \Pi_k(\widetilde{H}_D)}{\partial \delta}\rho_0\Pi_k(\widetilde{H}_D) \, |\mathrm{OUT}\rangle\end{aligned}$$

provides a measure of the sensitivity of the asymptotic fidelity to a parameter variation of size δ structured as S_{H_D}. To calculate $\frac{\partial \Pi_k(\widetilde{H}_D)}{\partial \delta}$ we assume that Π_k is the projector onto a 1-dimensional eigenspace, $\Pi_k(\widetilde{H}_D) = |v_k\rangle \langle v_k|$, so that

$$\frac{\partial \Pi_k(\widetilde{H}_D)}{\partial \delta} = \left| \frac{\partial v_k}{\partial \delta} \right\rangle \langle v_k| + |v_k\rangle \left\langle \frac{\partial v_k}{\partial \delta} \right|,$$

where $\{v_k\}_{k=1}^N$ are the eigenvectors of $\widetilde{H}_D$. We then calculate the derivatives of the eigenvectors in accordance with [19] (see also [20]) and present the method as applied to our case in Appendix B.

The logarithmic sensitivity of the error $\varepsilon_\infty = 1 - p_\infty$ can be written in terms of the preceding sensitivity:

$$\left| \frac{1}{\epsilon_\infty} \frac{\partial \epsilon_\infty}{\partial \delta} \right| = - \frac{2\Re \sum_k \langle \mathrm{OUT}| \frac{\partial}{\partial \delta} \Pi_k(\widetilde{H}_D)\rho_0\Pi_k(\widetilde{H}_D) |\mathrm{OUT}\rangle}{1 - \langle \mathrm{OUT}|\rho_\infty|\mathrm{OUT}\rangle}. \tag{26}$$

In the same spirit as [3] and [4], this logarithmic sensitivity of the error will be used in the sequel to assess whether the D-controller is "classical," or "anti-classical." By "anti-classical," we mean that the error and its log-sensitivity are concordant, or positively correlated, which goes against the classical limitations.

VI. Robustness & Robust performance

Here, instead of asymptotic or long-term average error $1 - p_\infty$, we look at the $z(t)$ error of Sec. IV, measured as $\hat{z}(\epsilon > 0)$, as already justified in Sec. IV-B. The advantage of such measure is that it picks up some transients in addition to some steady state components.

A. Robustness

Any perturbation of the Hamiltonian $\Delta_{H_D} = \delta S_{H_D}$ maps linearly via (17) to a perturbation of Bloch operator A_D, which we shall write as $A_D + \delta S_{\mathtt{H_D}}$. $S_{\mathtt{H_D}}$ transforms in the same manner as H and D

$$S_{\mathtt{H_D}\,kl} = \mathrm{Tr}\left(\jmath S_{H_D}[\sigma_k, \sigma_l]\right). \tag{27}$$

As dephasing acts in the Hamiltonian basis in our model, Hamiltonian perturbations also result in perturbations of the interaction with the environment. The dependence between the Hamiltonian and the Lindbladian uncertainty [11], [12] presents an added difficulty. Specifically, the perturbation of the decoherence operator Δ_{V_D} must be a solution to the equation

$$[H_D + \Delta_{H_D}, V_D + \Delta_{V_D}] = 0, \tag{28}$$

as the perturbed dephasing operator must commute with the perturbed Hamiltonian.

The solution to this equation is expressible as a power expansion in δ and restricting to first order (although not in the spirit of general μ-analysis) results in a Lyapunov equation for the coefficient S_{V_D} of δ. Retaining the solution $\Delta_{V_D} = \delta S_{V_D}$, another problem is that the mapping $\Delta_V \mapsto \Delta\mathtt{L}$ is nonlinear as seen from (17). However, if the perturbation is small enough, it can be approximated by

$$\begin{aligned}\Delta\mathtt{L}_{k\ell} =& \mathrm{Tr}(\Delta_{V_D}\sigma_k V_D \sigma_\ell) + \mathrm{Tr}(V_D\sigma_k\Delta_{V_D}\sigma_\ell) \\ &- \tfrac{1}{2}\mathrm{Tr}((V_D\Delta_{V_D} + \Delta_{V_D}V_D)\{\sigma_k, \sigma_\ell\}).\end{aligned} \tag{29}$$

Splitting Δ_{V_D} as δS_{V_D}, the resulting perturbation of $\mathtt{L}$ can trivially be written as $\delta S_{\mathtt{L}}$.

Thus the dynamics for a perturbation of the Hamiltonian or the bias field together with the resulting perturbation of the decoherence is of the form

$$\dot{\boldsymbol{s}} = (\bar{A}_{\mathtt{D}} + \delta S)\boldsymbol{s}, \tag{30}$$

where $S = S_{\mathtt{H_D}} + S_{\mathtt{L}}$, up to first order.

B. Robust performance: μ-analysis

If the system is initially prepared in a known quantum state and the dynamical generators are known, then the state of the system is implicitly known as it can be calculated without performing any further measurements on the system. The reliance on model-based feedback, however, implies that the robustness of the system with regard to perturbations of the dynamical generators or the initial state is crucial. This is the *performance* problem, that is, make the design insensitive to initial state errors. Here we look at *robustness* of this performance, whether the response to initial state errors is robust against coupling and bias field errors.

Since the controllers have already been designed [2], we absorb the controller $\mathtt{D}$ in the dynamics, and consider the incremental dynamics resulting from an initial state preparation error $d\boldsymbol{s}(0)$:

$$\begin{aligned}d\dot{\boldsymbol{s}}(t) &= (\bar{A}_{\mathtt{D}} + \delta S)d\boldsymbol{s}(t), \quad d\boldsymbol{s}(0) = w, \\ dz(t) &= \bar{C}d\boldsymbol{s}(t),\end{aligned} \tag{31}$$

where the affine term in (24) disappears in the incremental dynamics. The latter consists in a "nominal" dynamics $\bar{A}_{\mathtt{D}}$ and an uncertain dynamics δS, with δ and S the size and the structure, resp., of the perturbation. As such, $dz(t)$ is the effect of the initial state preparation error on the generalized error $z(t)$ of Sec. IV and subject to the uncertainties δS.

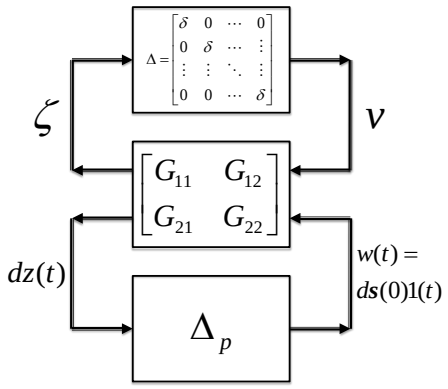

Fig. 1: Classically inspired robust performance design showing a fictitious perturbation Δ_p feedback from performance output to disturbance input

Consider the perturbed open-loop system and apply the matrix inversion lemma:

$$\begin{aligned}\left(sI - \bar{A}_{\mathfrak{D}} - \delta S\right)^{-1} &= \Phi + \Phi\delta(I - S\Phi\delta)^{-1}S\Phi, \\ (\Phi := (sI - \bar{A}_{\mathfrak{D}})^{-1}&).\end{aligned} \tag{32}$$

The right hand side of the above allows us to express the perturbation δS as a diagonally structured feedback as shown in Fig. 1, where

$$\begin{pmatrix} G_{11} & G_{12} \\ G_{21} & P_{22} \end{pmatrix} = \begin{pmatrix} S\Phi & S\Phi \\ \bar{C}\Phi & \bar{C}\Phi \end{pmatrix}. \tag{33}$$

Indeed, temporarily disregarding the fictitious feedback Δ_p, it is easily found that the transfer matrix from $w = d\boldsymbol{s}(0)$ to dz is

$$\begin{aligned} T_{dz,w} &= G_{22} + G_{21}\Delta(I - G_{11}\Delta)^{-1}G_{12} \\ &= C\left(sI - \bar{A}_D - \delta S\right)^{-1}. \end{aligned} \tag{34}$$

(See [3], [8] for details.) Since the preparation error once set remains constant, and as more formally justified in Sec. IV-B, we set $s = \epsilon > 0$, and the figure of merit is set as $\|T_{dz,w}(\epsilon)\|$, where $\|\cdot\|$ denotes the maximum singular value.

Next, we close the dz to w loop with a fictitious feedback Δ_p so as to bound $\|T_{dz,w}(s)\|$ using stability margin concepts. To derive such a bound under physical parameter variation $\Delta = \delta I$, define $\boldsymbol{\Delta}$ to be the augmented $\boldsymbol{\mathcal{D}}$-structured perturbation

$$\boldsymbol{\Delta} = \begin{pmatrix} \Delta & 0 \\ 0 & \Delta_p \end{pmatrix}. \tag{35}$$

$\boldsymbol{\Delta}$ is structured in two different ways: first of all it has block diagonal structure and secondly Δ is diagonal, δI. Traditionally, there is no a priori structure on Δ_p, except that its size should be compatible with the dimension of $d\boldsymbol{z}$ and $\boldsymbol{w}$. Define

$$\mu_{\boldsymbol{\mathcal{D}}}(G) = \frac{1}{\min\{\|\boldsymbol{\Delta}\| : \boldsymbol{\Delta} \in \boldsymbol{\mathcal{D}}, \det(I - G\boldsymbol{\Delta}) = 0\}}. \tag{36}$$

Next, observe that

$$\det(I - G(s)\boldsymbol{\Delta}) = \det(I - G_{11}(s)\Delta)\det\left(I - T_{dz,w}(s)\Delta_p\right). \tag{37}$$

Since the uncertainty Δ does not affect closed-loop stability guaranteed by decoherence, $\det(I - G_{11}(s)\Delta) \neq 0$, $\forall \Re s \geq 0$, $\forall \Delta \neq 0$. Hence $\det(I - G(s)\boldsymbol{\Delta}) = 0$ iff $\det\left(I - T_{dz,w}(s)\Delta_p\right) = 0$. The latter together with [6, Th. 10.8] yields

Theorem 2: $\|T_{dz,w}(s)\| \leq B$ for $\|\Delta\| < 1/B$ iff $\mu_{\boldsymbol{\mathcal{D}}}(G(s)) \leq B$.

Remark 1: Traditionally in robust control [6], w is an arbitrary extraneous disturbance, justifying the lack of structure of Δ_p except for its size that has to be compatible with dz and w. The problem is that, as shown in Appendix C, the very specific setup of the problem makes Δ_p structured in a way not supported by *mussv* of Matlab. Therefore, we had to relax Δ_p to be complex, fully populated. Now, observe the following string of inequalities:

$$\begin{aligned} &\text{mussv upper bound}\left(\mu_{\boldsymbol{\mathcal{D}}}(G)\right) \\ &\geq \frac{1}{\min\left\{\left\|\boldsymbol{\Delta} = \begin{pmatrix} \delta I & 0 \\ 0 & \Delta_p \end{pmatrix}\right\| : |I - G\boldsymbol{\Delta}| = 0, \Delta_p \in \mathbb{C}^{nr\times nc}\right\}} \\ &\geq \frac{1}{\min\left\{\left\|\boldsymbol{\Delta} = \begin{pmatrix} \delta I & 0 \\ 0 & \Delta_p \end{pmatrix}\right\| : |I - G\boldsymbol{\Delta}| = 0, \Delta_p \in \mathcal{D}_p\right\}}, \end{aligned}$$

where the structure $\mathcal{D}_p$ is defined in Appendix C and $|\cdot|$ is a short for $\det(\cdot)$. Our computational results based on a complex, fully populated Δ_p, although conservative, will still be correct as the $\mu_{\boldsymbol{\mathcal{D}}}$ computed on the basis of an unstructured Δ_p will be an upper bound for the $\mu_{\boldsymbol{\mathcal{D}}}$ computed for a structured Δ_p.

VII. Simulations

To numerically investigate the robust performance and sensitivity of the system relative to parameter variations, we consider test cases of rings with XX-coupling ranging in size from $N = 3$ to $N = 6$, restricted to the single excitation subspace. For each N, a set of eigenvalues $\{c_k\}_{k=1}^N$ of the quantum jump operator V_D were selected by random draw of the uniform distribution over $[0, 1]$, as shown in Table I. Note that the bias towards positive values is not an issue, as the crucial parameters are the $\gamma_{k\ell}$'s, which can be rewritten as $-(1/2)((c_k - 0.5) - (c_\ell - 0.5))^2$, as if the c_k's were zero mean. For each ring a set of time-invariant static bias fields D was computed by numerically maximizing the probability of transport over a small time window about a given time t_f,

$$p_{t_f} = \left|\sum_{k\in\mathcal{K}} e^{-t_f(\jmath\lambda_k)} \langle \mathrm{OUT}| \Pi_k(H_D) |\mathrm{IN}\rangle\right|^2, \tag{38}$$

or a larger window in case of localization, as described in previous work [1] with data taken from [21]. The optimization was performed for the ideal Hamiltonians (13) and without decoherence. Excitation transfers from the initial state $|\mathrm{IN}\rangle = |1\rangle$ to a final state $|\mathrm{OUT}\rangle = |n\rangle$ for $n = 1, 2, \ldots, \lceil \frac{N}{2} \rceil$ were considered. For each transfer problem 1000 to 2000 independent controllers were calculated and ordered by increasing error. Here $|n\rangle = \boldsymbol{e}_n$ and we identify the excitation localized at a spin n with the nth natural basis vector of the single excitation subspace.

TABLE I: Eigenvalues of quantum jump operator V_D. For each N, the c_k's are draws from a uniform distribution over $[0, 1]$.

N	c_1	c_2	c_3	c_4	c_5	c_6
6	0.4228	0.5479	0.9427	0.4177	0.9831	0.3015
5	0.4050	0.2517	0.5811	0.8083	0.0504	
4	0.5342	0.4539	0.7924	0.2188		
3	0.4914	0.89170	0.7315			

Note that (38) can be rewritten as

$$\sum_{k,\ell} e^{-\jmath\omega_{k,\ell}t_f}\langle \mathrm{OUT}|\Pi_k|\rho(t_f)|\Pi_\ell|\mathrm{OUT}\rangle$$
$$= \langle \mathrm{OUT}|\rho(t_f)|\mathrm{OUT}\rangle \overset{t_f\to\infty}{=} \rho_\infty.$$

Therefore, the finite-time optimized D-controllers in the database [21] are relevant to the near steady-state optimization done here if t_f is large enough. Regardless of this slight discrepancy, it is argued that the database [21] provides a variety of controllers providing a variety of levels of performance against which discordance & concordance among the various figures of merit can be assessed.

A. *Effect of Hamiltonian uncertainties and control errors*

Operating in this single excitation subspace basis, we retain the structure of S_{H_D} as presented in (13), with the J_{mn}'s normalized to 1. Identifying spin $N+1$ with 1 and spin 0 with N for simplicity, the structured perturbation S_{H_D} for coupling uncertainty between spin n and $n+1$, is an $N\times N$ matrix of all zeros, save for a 1 in the $(n, n+1)$ and $(n+1, n)$ positions. For spillage of the bias field at spin n, S_{H_D} is an $N\times N$ matrix with a -1 at (n, n) and $\frac{1}{2}$ in the $(n+1, n+1)$ and $(n-1, n-1)$ entries, multiplied by the strength of the bias field D_k. This yields the perturbed Hamiltonian as $\widetilde{H}_D = H + D + \delta S_{H_D} = H_D + \delta S_{H_D}$.

To ensure commutativity of the Lindblad operator with the perturbed Hamiltonian we enforce Eq. (28). Retaining only terms up to first order in δ yields $[S_{V_D}, H_D] = [V_D, S_{H_D}]$, which we solve for S_{V_D} as

$$\mathrm{Vec}(S_{V_D}) = (I\otimes H_D - H_D\otimes I)^\dagger \mathrm{Vec}([V_D, S_{H_D}]), \quad (39)$$

where Vec denotes the vectorization of an $N\times N$ matrix by stacking together the columns, I is the identity matrix in the single excitation subspace and $M^\dagger$ indicates the Moore-Penrose inverse of the matrix M.

Having solved (39), equivalently (28), we then solve (29) for the perturbed system, and construct the state space system (30).

We note that $\Pi_k\dot{\rho}(t)\Pi_k = 0$, i.e., $\bar{A}_D$ has $N-1$ eigenvalues at zero following the Bloch vectorization. Thus, computation of $\Phi = (sI - \bar{A}_D)^{-1}$ at $s = 0$ to reflect the constant input $|\mathrm{IN}\rangle$ as in [3] presents obvious issues. To obviate this roadblock, and as justified in Sec. II-C, we choose a small value of $s = 10^{-2}$ to allow for numerical simulation and production of results (25). As shown in Figs. 2 and 3, lowering the value of s does not change the overall trend in the relation between the probability of transfer and μ but does have an inverse effect on the magnitude of μ, as anticipated by the 0-eigenvalues of $\bar{A}_\mathbf{D}$.

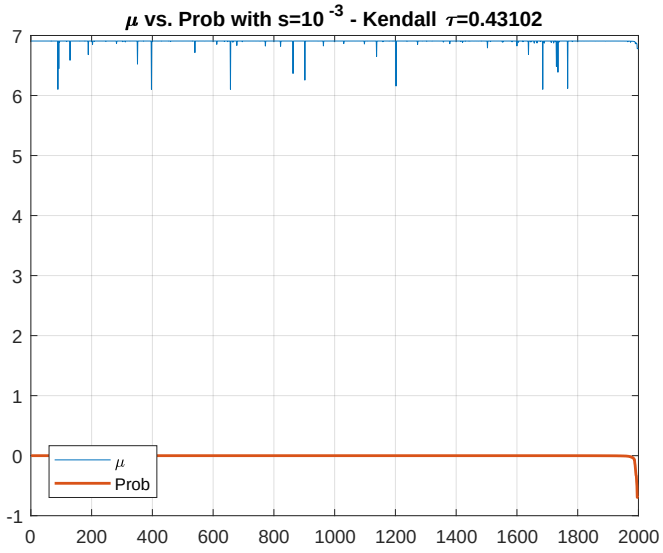

Fig. 2: Probability of transfer versus μ for coupling uncertainty between spins 1 and 2 in a $|1\rangle \to |1\rangle$ "transfer" (localization) in a 5-ring evaluated at $s = 10^{-3}$.

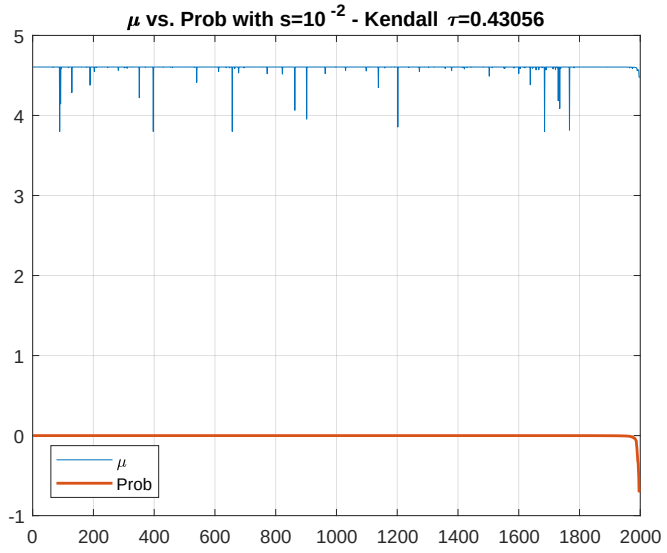

Fig. 3: Same transfer and perturbation set-up as in Fig. 2 but evaluated at $s = 10^{-2}$. Note that though the magnitude of μ decreases with the increase in frequency the overall trend remains the same with a difference in the Kendall t of only 0.00046.

With these simplifying assumptions and with the understanding that we are using the reduced system, we construct the generalized plant in equations (32)-(33) where Φ and S are the $(N^2-1)\times(N^2-1)$ and $\bar{C}$ is the $(N-1)\times(N^2-1)$ matrices described in Sec. IV. From the way we derived S_{V_D} in the single excitation subspace we see that the same value of δ multiplies both S_H and S_L, and so combining these two terms into a single structure matrix S allows us to use the simplified single-perturbation set-up of Section VI-B from

which we can absorb the controller into the plant and construct the block-diagonal of (35) after closing the loop between $dz(t)$ and $ds(0)$ with the fictitious, full $(N^2-1)\times(N-1)$ perturbation matrix Δ_p. From here, Matlab's *mussv* command can be used to evaluate the upper bound on $\mu_{\boldsymbol{\mathcal{D}}}(G)$ where G is the block 2×2 system of (33) with the loop closed by $\boldsymbol{\Delta}$ and $\boldsymbol{\mathcal{D}}$ indicates all matrices with the same block-diagonal structure as $\boldsymbol{\Delta}$.

VIII. Statistical Analysis and Results

A. Statistical Analysis and Hypothesis Testing

To determine whether a specific perturbation of the coupling uncertainties or bias fields within a given excitation transfer displays classical or anti-classical trends we rely on statistical analysis to decide on the level of classicality. We first associate performance with the probability (squared fidelity) of a successful transfer of the excitation from the initial spin to the target spin. As well known, from the classical control perspective, we expect those controllers with the best performance (squared fidelity near unity) to display the least amount of robustness. As discussed at length in [1], [3], [4], [8], this trend is reversed in the coherent regime. Here, we show that decoherence recovers the classical trend.

We look for indications of the lack of robustness in two ways.

First, from the robust performance condition $\mu_{\boldsymbol{\mathcal{D}}}(G)\leq B$ for all structured perturbations such that $\|\Delta\|<\frac{1}{B}$ we see that a large value of μ indicates a small tolerance in the size of the allowable perturbations and vice versa for small μ. So, we can associate smaller values of μ with increased robustness to parameter variation and thus expect to see a positive correlation between probability and μ. Regarding the log-sensitivity we rely on the classical identity $I=S(s)+T(s)$ where S and T are the sensitivity and complementary-sensitivity transfer functions, respectively. It is well known that $S(s)$ provides the transfer function from the reference signal to error, and thus we associate increased S with an increase in error or decrease in performance. Through the relation $S^{-1}(dS)=(dL)L^{-1}T$ we can then associate the sensitivity of $S(s)$ (or log-sensitivity) to variations in the plant L with the complementary sensitivity function T, i.e., we should see the classical log-sensitivity decrease with the increase in error (drop in performance). In short, we anticipate a positive correlation between both μ and the log-sensitivity with the designated performance measure, the probability of transfer. Furthermore, we anticipate a positive correlation between both μ and the log-sensitivity as a measure of consistency.

To ensure an objective treatment of the trend analysis, we use the Kendall τ [22] to measure rank correlation between the metrics of interest and run a single-tailed hypothesis test. We take the null hypothesis as H_0 : no rank correlation between the metrics under consideration or $\mu_\tau=0$ where μ_τ indicates the mean value of the Kendall τ. As detailed in [22] with a sample size greater than 10, the distribution of the Kendall τ rapidly assumes a normal distribution with a mean of zero and standard deviation given by $\sigma_\tau=\sqrt{\frac{2(2M+5)}{9M(M-1)}}$. With a sample size of $M=2000$ for each test iteration we can thus use the normal test statistic $Z_\tau=\frac{\tau}{\sigma_\tau}$ in a one-tailed hypothesis test to indicate the presence or absence of positive rank correlation between the metrics of interest. Since we are looking for instances of classical behavior or positive correlation we establish the alternative hypothesis as H_1 : positive correlation between the metrics or $\mu_\tau>0$. We establish the probability of Type I error α as 0.05 which for our sample size requires value of $Z_\tau\geq 1.645$ (or a raw value of $\tau\geq 0.0245$) to demonstrate concordance between the metrics and indicate a strong case for classicality as $F(Z_\tau)=1-p_\tau>1-\alpha=0.95$ under this condition and where $F(Z)$ is the standard normal cdf. Likewise, a value of $Z_\tau<1.645$ (or a raw value of $\tau<0.0245$), while not necessarily showing strong anti-classical behavior, does not support the trend of classicality. With regard to the power of the test, if we assume that the true mean of the distribution is the observed value of τ, then with $\alpha=0.05$, we require a value of $Z_\tau\geq 2.486$ (or a raw value of $\tau\geq 0.03710$) in order to support a strong classical trend with a power $1-\beta\geq 0.80$.

For each ring from $N=3$ through $N=6$, each transfer for which data was available for the given ring, and each case of either bias spillage or coupling uncertainty we apply the given hypothesis test to determine whether under the specific size, transfer, and uncertainty conditions we observe classical or anti-classical behavior. This provides for 94 test cases, half specific to bias spillage and the other half involving coupling uncertainty, in which to determine the relation between μ and probability, log-sensitivity and probability, and μ and log-sensitivity. To make the results more concise, we use Stouffer's method [23], [24] to combine the results of the N possible coupling uncertainty variations or bias spillage variations within each transfer in a ring of size N. By Stouffer's method, given M independent trials resulting in Z-scores of $Z_{\tau_k}=\frac{\tau_k}{\sigma_\tau}$ we can get an aggregate Z-score $Z_s=\sum_{m=1}^{M}\frac{Z_{\tau_k}}{\sqrt{M}}$ and resulting aggregate $p_s=1-F(Z_s)$ to allow for application of the hypothesis test described above to the overall level of classicality or lack thereof observed in a specific transfer [23]. With regard to independence of the various test runs, we note that all conditions remain the same, save for the location of perturbation under consideration within each specific test case, and can thus justify the claim of independence between simulation test cases within a specific ring size and transfer.

B. Coupling Uncertainty Results

We see the overall trend for the case of coupling uncertainty in Table II. As exhibited in the table, the relationship between probability of transfer and $\mu_{\boldsymbol{\mathcal{D}}}$, as well as probability and log-sensitivity, is overwhelmingly strongly classical, indicating that the decoherence model used in the simulations enforces more classicality between these two metrics than what is observed in the case of unitary evolution of the system. Though not as strongly classical we do note an overall positive trend across all transfers and N's between probability and log-sensitivity. Of interest is that all cases of non-classical behavior observed are due to a $|1\rangle\rightarrow|2\rangle$ transfer of the excitation while the remaining transfers remain strongly classical. Further

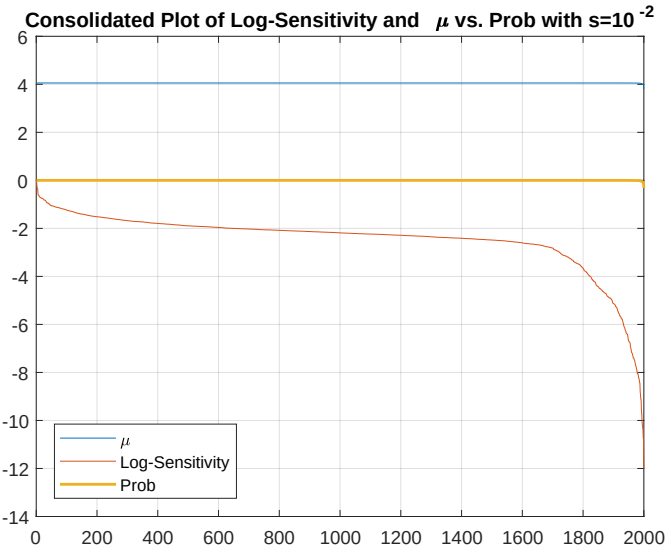

Fig. 4: Plot of μ and log-sensitivity versus probability for a 3-ring undergoing localization of the excitation with coupling uncertainty between spins 2 and 3

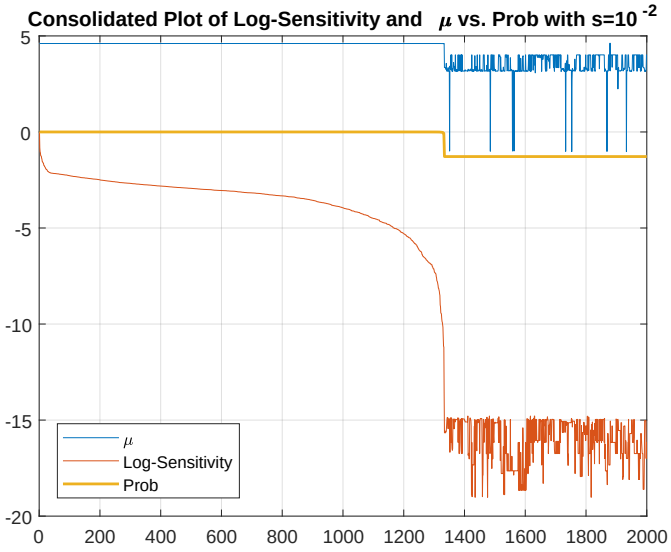

Fig. 5: Plot of μ and log-sensitivity versus probability for a 6-ring undergoing localization of the excitation with coupling uncertainty between spins 1 and 2.

investigation into the cause of this lack of classicality specific to this transfer is certainly warranted.

Another interesting aspect of these results is that the case of a $|1\rangle \rightarrow |1\rangle$ "transfer" or localization about a specific spin is overwhelmingly classical under the decoherence model while in the case of unitary evolution we expect this localization to be highly anti-classical. Fig. 4 shows the results for a 3-ring undergoing localization with uncertainty in the 1-2 spin coupling. We note the strong concordance between both log-sensitivity and probability and $\mu_{\mathcal{D}}$ and probability both visually and with a Kendall τ of unity between both metrics and probability of transfer. Fig. 5 reveals the same trend for the case of localization in a 6-ring with 1-2 coupling uncertainty. Though the plots are noisier than the preceding one, the strong positive trend is still clearly visible. These positive trends are borne out by a Kendall τ of 0.7008 for the μ-probability trend and 0.8898 for that of the log-sensitivity-probability relation.

In opposition to the cases of agreement with classical behavior, we see in Fig. 6 the non-classical behavior resulting from a $|1\rangle \rightarrow |2\rangle$ transfer in a 6-ring with coupling uncertainty between spins 3 and 4. Here we note that μ trends strongly in the negative direction from the probability with a Kendall τ of -0.3063. The trend between log-sensitivity and probability, however, remains strongly classical with a Kendall τ of 0.7181.

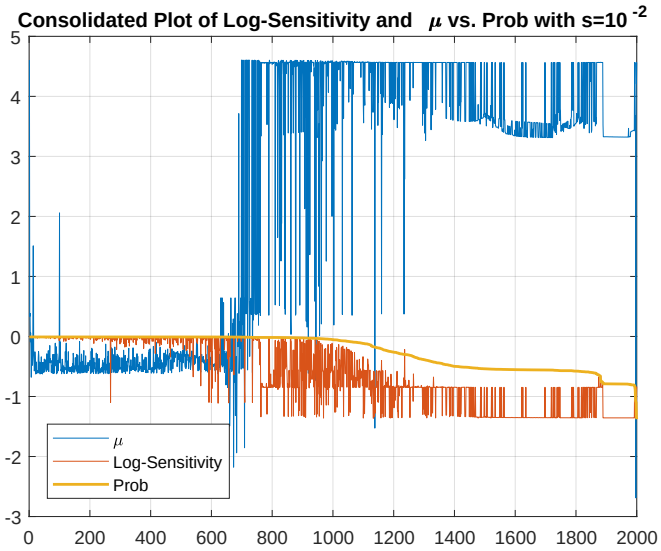

Fig. 6: Consolidated plot of metrics for a 6-ring $|1\rangle \rightarrow |2\rangle$ transfer with coupling uncertainty between spins 3 and 4. Note the anti-classical behavior of μ versus probability juxtaposed with the classical trend between probability and log-sensitivity.

C. Bias Spillage Results

The results for the trends when the perturbation in the system results from bias spillage are summarized in Table III. We can immediately note that the trend between $\mu_{\mathcal{D}}$ and probability does not support strong classical behavior in a plurality of cases, especially regarding the transfers in a 5-ring. For the log-sensitivity-probability trend, we note the same level of non-classical behavior, but no pattern as in the coupling uncertainty with $|1\rangle \rightarrow |2\rangle$ transfers.

From Table III, we can deduce that the only cases that support strong classical behavior in both $\mu_{\mathcal{D}}$ and log-sensitivity are those that involve localization of the excitation. This is not a uniform trend, as localization in the 5-ring still produces a non-classical trend between $\mu_{\mathcal{D}}$ and probability, however it does hold for all other cases considered. We can see this classical trend in Fig. 7 showing the results of localization in a 4-ring with bias spillage on spin 1. Here the Kendall τ for

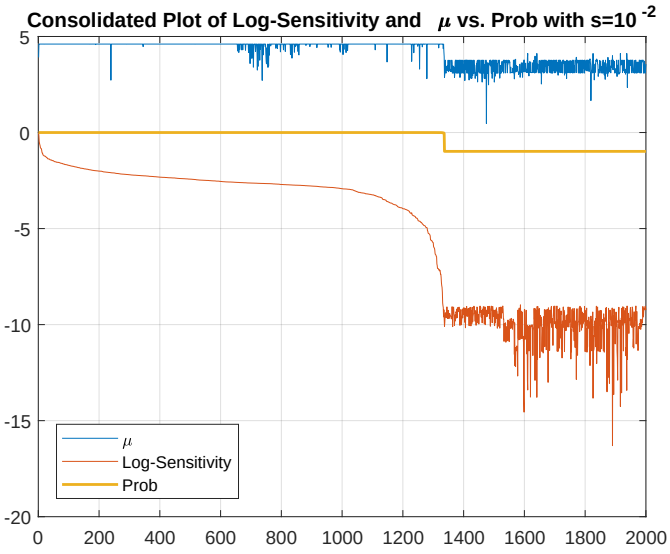

Fig. 7: Localization of the excitation at spin 1 for a 4-ring with bias spillage on spin 1. Here we can see classical behavior for both μ and the log-sensitivity which is not the norm in the bias spillage test cases.

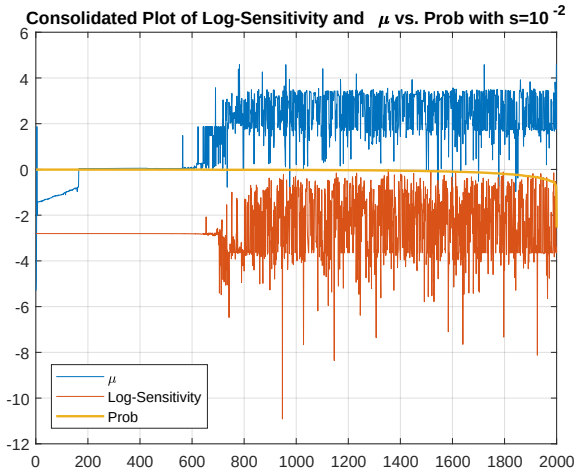

Fig. 8: Consolidated plot for a $|1\rangle \rightarrow |2\rangle$ transfer in a 5-ring with bias spillage on spin 3. Here we can clearly observe a negative trend between μ and probability (Kendall $\tau = -0.5294$) while the log-sensitivity and probability display an almost neutral trend (Kendall $\tau = 0.0365$).

the $\mu_{\mathcal{D}}$-probability trend is 0.6913 and, even more strongly, we can verify the positive correlation between log-sensitivity and probability of 0.9240. More characteristic of the results observed for bias spillage are those depicted in Fig. 8. This provides a plot of the results for a $|1\rangle \rightarrow |2\rangle$ transfer in a 5-ring with bias spillage on spin 3.

In addition to anti-classical cases such as that in Fig. 8, we also note that within a given transfer for a specific ring, the results can vary dramatically based on the location of the bias spillage. For example, we consider the case of a 5-ring and a $|1\rangle \rightarrow |3\rangle$ transfer. If we have the bias spillage on

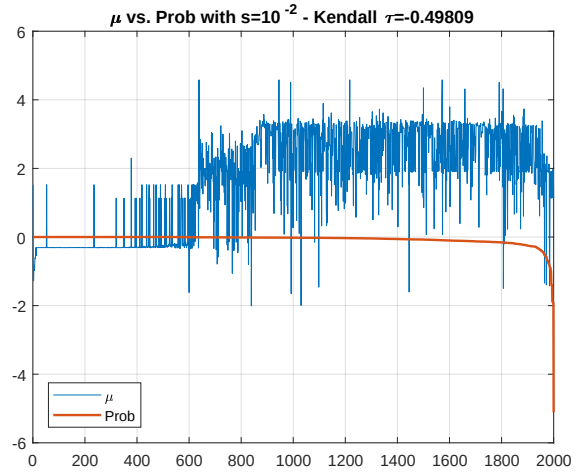

Fig. 9: Plot of trends for a $|1\rangle \rightarrow |3\rangle$ in a 5-ring with bias spillage on spin 1. Here we see a clear increase in μ (reduction in robustness) as the probability decreases.

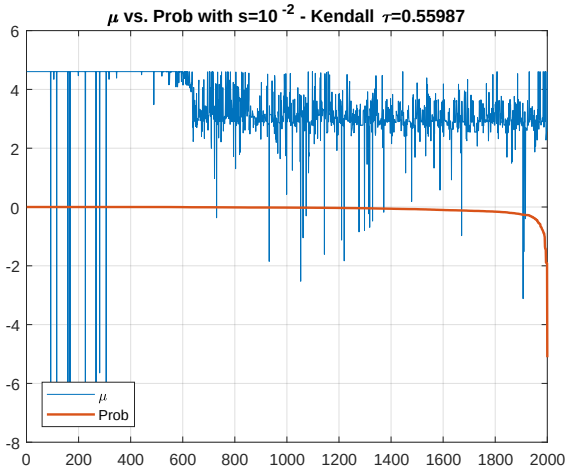

Fig. 10: Plot of μ and probability for a $|1\rangle \rightarrow |3\rangle$ transfer in a 5-ring with spillage on spin 2. In comparison with Fig. 9, we see completely opposite trends between the metrics with the change in the perturbation from one spin to its neighbor.

spin 1 then we note a non-classical μ-probability trend of $\tau = -0.4981$ and a classical trend for log-sensitivity and probability of $\tau = 0.1709$. However, with the spillage located on spin 2, the behavior is totally opposite with a Kendall τ of 0.5595 for μ and probability and that of -0.3217 for the trend between log-sensitivity and probability. Such drastic changes in the trends between the metrics indicates an overall lack of robustness to bias spillage with the current model.

D. Correlation Between μ and Log-Sensitivity

As a measure of consistency in the results, we also examine the relation between $\mu_{\mathcal{D}}$ and the log-sensitivity as both give a measure of how resistant the system's performance is to perturbations within the parameters, though on different scales. Regardless, we expect those systems with a small value of

$\mu_{\mathcal{D}}$ to be more robust as they allow for a larger $\|\Delta\|$ before violating the robust performance criteria and expect that this larger value of robustness will correlate with a smaller value of the log-sensitivity as the latter measures the change in performance to differential changes in the parameter values. To examine this correlation, we use the same hypothesis test as in the previous sections with an α of 0.05 to determine whether the data provide proof of strong correlation between the two metrics. We apply the hypothesis test using the Kendall τ for each possible single perturbation within the allowable transfers for rings from size $N = 3$ to $N = 6$ and then apply Stouffer's method to consolidate the results for each transfer in the separate cases of coupling uncertainty and bias spillage. Table IV summarizes the results of the hypothesis test and indicates that in 80% of the transfers we see the expected strong positive correlation between μ and the log-sensitivity.

IX. Conclusions

This study involves sensitivity and robust performance of controllers optimized for fidelity of transfers in spin rings under decoherence.

There are 3 kinds of uncertainties considered here: coupling uncertainty, bias spillage, and initial state preparation errors. While decoherence is another source of uncertainty, it is not treated as an uncertainty in the sense that the effect of its strength on fidelity, investigated in [7], is not considered here; rather, our objective is to show that the mere presence of decoherence causes an anti-classical to classical transition. There are 3 quality metrics involved: fidelity, sensitivity, and μ. Assessing results with different metrics under different kind of uncertainties makes drawing conclusions a bit challenging. Nevertheless, if we look at Tables II-IV patterns do emerge.

To make objective, quantitative statements as to whether figures of merit are concordant or discordant, we use the Kendall τ to assess consistency ($\tau = 1$) or inconsistency ($\tau = -1$) between different metrics in a sample of experiments specified by a common number N of spins, a common transfer, and a common uncertainty structure (coupling uncertainty or bias spillage) for varying location of the uncertainty along the ring. We then combine the various τ's for the various sample of experiments in a consolidated Stouffer p_s indicating consistency for $p_s = 0$ and inconsistency for $p_s = 1$, almost in a "zero-one" law. Table IV shows consistency between the log-sensitivity and the μ for coupling uncertainties, even though the two metrics do not quite pick up the same "sensitivity:" the μ is a measure of the robustness of the response to an initial preparation error to coupling or bias spillage uncertainty, while the classical sensitivity does not take the initial preparation error into consideration and merely assess sensitivity of fidelity to coupling and bias spillage errors.

Our overall claim of emergence of classicality under decoherence is obvious from Table II, where the consolidated Stouffer p_s shows classical consistency between, on the one hand, the fidelity and μ and, on the other hand, the fidelity and log-sensitivity.

Finally, regarding bias spillage errors, there is no clear pattern—except for the case of localization where classicality is obvious from Tables III and IV for $1 \to 1$ "transfers." Remember that in the coherent case, localization is the best example of anti-classical behavior and it appears that decoherence makes localization flip from anti-classical to classical behavior, again reinforcing our claim of emergence of classicality under decoherence.

As future work, it is our intent to combine the present results with those of [7] in a multi-dimensional study involving 3-fold uncertainty: decoherence, coupling errors, and bias spillage.

References

[1] S. Schirmer, E. Jonckheere, and F. Langbein, "Design of feedback control laws for spintronics networks," *IEEE Transactions on Automatic Control*, vol. 63, no. 8, pp. 2523–2536, August 2018, available at arXiv:1607.05294.

[2] F. Langbein, S. Schirmer, and E. Jonckheere, "Time optimal information transfer in spintronics networks," in *IEEE Conference on Decision and Control*, Osaka, Japan, December 2015, pp. 6454–6459.

[3] E. Jonckheere, S. Schirmer, and F. Langbein, "Structured singular value analysis for spintronics network information transfer control," *IEEE Transactions on Automatic Control*, vol. 62, no. 12, pp. 6568–6574, December 2017, available at arXiv:1706.03247v1 [quant-ph] 10 Jun 2017.

[4] ——, "Jonckheere-Terpstra test for nonclassical error versus log-sensitivity relationship of quantum spin network controllers," *International Journal of Robust and Nonlinear Control*, vol. 28, no. 6, pp. 2383–2403, April 2018, available at arXiv:1612.02784 [math.OC].

[5] P. W. Anderson, "Absence of diffusion in certain random lattices," *Physical Review*, vol. 109, no. 5, pp. 1492–1505, March 1958.

[6] K. Zhou and J. C. Doyle, *Essentials of robust control*. Upper Saddle River, NJ: Prentice Hall, 1998.

[7] S. Schirmer, E. Jonckheere, S. O'Neil, and F. Langbein, "Robustness of energy landscape control for spin networks under decoherence," in *IEEE CDC*, Miami Beach, FL, 2018, pp. 6608–6613.

[8] S. O'Neil, E. Jonckheere, S. Schirmer, and F. Langbein, "Sensitivity and robustness of quantum rings to parameter uncertainty," in *IEEE CDC*, Melbourne, Australia, December 2017, pp. 6137–6143, available at arXiv:1708.09649v1.

[9] B. L. Hu, "Gravitational decoherence, alternative quantum theories and semiclassical gravity," *Journal of Physics: Conference series*, vol. 504, pp. 1–15, 2014.

[10] W. H. Zurek, "Decoherence and the transition from quantum to classical," *Physics Today*, pp. 36–44, October 1991.

[11] D. D'Alessandro, E. Jonckheere, and R. Romano, "Control of open quantum systems in a bosonic bath," in *54th IEEE Conference on Decision and Control (CDC)*, Osaka, Japan, December 2015, pp. 6460–6465, available at `http://ee.usc.edu/ jonckhee`.

[12] D. P. D'Alessandro, E. Jonckheere, and R. Romano, "On the control of open quantum systems in the weak coupling limit," in *21st International Symposium on the Mathematical Theory of Networks and Systems (MTNS)*, Groningen, the Netherlands, July 7-11 2014, pp. 1677–1684.

[13] Z. H. Wang, Y. J. Ji, Y. Li, and D. L. Zhou, "Dissipation and decoherence induced by collective dephasing in a coupled-qubit system with a common bath," *Phys. Rev. A*, vol. 91, p. 013838, Jan 2015. [Online]. Available: http://link.aps.org/doi/10.1103/PhysRevA.91.013838

[14] E. Gluskin and S. Miller, "On the recovery of the time average of contionuous and discrete time functions from their Laplace and z-transform," 2011, arXiv:1109.3356v4 [math-ph].

[15] F. F. Floether, P. de Fouquieres, and S. Schirmer, "Robust quantum gates for open systems via optimal control: Markovian versus non-Markovian dynamics," *New Journal of Physics*, vol. 14, pp. 1–26, 2012, 073023.

[16] R. A. Bertlmann and P. Kramer, "Bloch vectors for audits," 2008, available at arXiv :0806.1174v1 [quant-ph] 6 June 2008.

[17] M. H. S. Amin and D. V. Averin, "Macroscopic resonant tunneling in the presence of low frequency noise," *Phys. Rev. Lett.*, vol. 100, p. 197001, May 2008. [Online]. Available: https://link.aps.org/doi/10.1103/PhysRevLett.100.197001

[18] D. P. L. Castrigiano and S. A. Hayes, *Catastrophe Theory*. Reading, MA: Addison-Wesley, 1993.

[19] F. Wei, "Efficient method for eigenvector derivatives with repeated eigenvalues," in *33rd Structures, Structural Dynamics, and Materials Conference*, Dallas, TX, 1992.

[20] N. van der Aa, "Computation of eigenvalue and eigenvector derivatives for a general complex-valued eigensystem," *Electronic Journal of Linear Algebra*, vol. 16, pp. 300–314, October 2007. [Online]. Available: https://www.emis.de/journals/ELA/ela-articles/articles/vol16_pp300-314.pdf

[21] F. C. Langbein, S. G. Schirmer, and E. Jonckheere, "Static bias controllers for XX spin-1/2 rings," July 3 2016, data set, `figshare`, DOI:10.6084/m9.figshare.3485240.v1.

[22] H. Abdi, "The Kendall rank correlation coefficient," in *Encyclopedia of measurements and Statistics*, N. Salkind, Ed. Thousand Oaks, CA: Sage, 2007.

[23] M. C. Whitlock, "Combining probability from independent tests: the weighted z-methods is superior to Fisher's approach," *J. Evol. Biol.*, vol. 18, pp. 1368–1373, 2005.

[24] K. Tsuyuzaki, "Stouffer.test: Stouffer weighted Z-score (inverse normal method)." [Online]. Available: https://www.rdocumentation.org/packages/metaSeq/versions/1.12.0/topics/Stouffer.test

[25] D. K. L. Oi and S. G. Schirmer, "Limits on the decay rate of quantum coherence and correlation," *Physical Review A*, vol. 86, pp. 012 121–1–012 121–7, 2012.

[26] V. Gorini, A. Kossakowski, and E. C. G. Sudarshan, "Completely positive dynamical semigroups of n-level systems," *Journal of Mathematical Physics*, vol. 17, no. 5, May 1976.

[27] S. G. Schirmer and A. I. Solomon, "Constraints on relaxation rates for N-level quantum systems," *Physical Review A*, vol. 70, pp. 022 107–1–022 107–13, 2004.

APPENDIX

A. Complete positivity

In this Appendix, we show that the simple Lindblad model,

$$L = V\rho V^\dagger - \frac{1}{2}\{V^\dagger V, \rho\},$$

is "physically realizable" in the sense that the induced decoherent dynamics is completely positive. Note that this model is slightly more general than the one of the main body (10), as the jump operator V is not restricted to be Hermitian. (For ease of the notation, we drop the subscript D.) Complete positivity can be shown as follows: Let $\{F_i\}_{i=1}^{N^2}$ be an orthonormal basis of the set of complex $N \times N$ operators over the complex field $\mathbb{C}$. We pick $N^2 - 1$ traceless operators and one operator (the N^2th one) proportional to the identity, $\frac{1}{\sqrt{N}} I_N$. Write

$$V = \sum_{i=1}^{N^2} \varphi_i F_i, \quad V^\dagger = \sum_{j=1}^{N^2} \varphi_j^* F_j^\dagger.$$

Then we find

$$L = \sum_{i,j=1}^{N^2} \varphi_i \varphi_j^* \left(F_i \rho F_j^\dagger - \frac{1}{2}\{F_j^\dagger F_i, \rho\} \right).$$

Now, let us absorb the contribution of $F_{N^2} = \frac{1}{\sqrt{N}} I_N$ in the Hamiltonian using the "gauge transformation" of [25] and we find the decoherence model

$$L = \sum_{i,j=1}^{N^2-1} \varphi_i \varphi_j^* \left(F_i \rho F_j^\dagger - \frac{1}{2}\{F_j^\dagger F_i, \rho\} \right),$$

where the F_i's are traceless operators. This is the Gorini, Kossakowski and Sudarshan model [26]. Following on that thread, since the matrix $\{\varphi_i \varphi_j^*\}_{i,j=1}^{N^2-1}$ is obviously positive semidefinite, by [26, Theorem 2.2], the dynamical map is completely positive.

To connect more explicitly with Sec. II-B, Eq. (9), we take $V = V^\dagger$ to commute with the Hamiltonian H, revert to the basis $\{\sigma_i\}_{i=1}^{N^2}$ of Hermitian operator, and observe the following:

$$\begin{aligned} V &= \sum_k c_k \Pi_k(H), \\ &= \sum_i \underbrace{\left(\sum_k c_k \varphi_{ki} \right)}_{\varphi_i} \sigma_i, \end{aligned}$$

where the $\{\varphi_{ki}\}_{i=1}^{N^2}$ are the coefficients of $\Pi_k(H)$ in the basis $\{\sigma_i\}_{i=1}^{N^2}$. Clearly any random sampling of the c_k's will result in a completely positive dynamics.

It should be observed that such a random sampling might not lead to a good sampling of the decoherence rates

$$\gamma_{k,\ell} = \frac{1}{2}(c_k - c_\ell)^2.$$

The problem is that a direct random sampling of the $\gamma_{k,\ell}$'s will not in general result in a completely positive dynamics and requires the "invert dephasing rate" test for realizability [25], [27], as was done in [7].

B. Derivation of Hamiltonian Eigenvector Derivatives

This short appendix is basically a summary of the procedure presented in [20] for the derivation of eigenvector derivatives for non-defective matrices.

As noted above, we use the process for calculating eigenvector derivatives as elucidated in [20]. To begin, let us define the matrices of interest as functions of the parameter δ, so that we have $\tilde{H}_D(\delta) = H + D + \delta S_{H_D}$. Now the eigenvalues and eigenvectors of the perturbed Hamiltonian are also functions of δ which we denote $\lambda_k(\delta)$ and $x_k(\delta)$ for $k = 1$ to N. Taking $\Lambda(\delta)$ as the diagonal matrix of eigenvalues and $X(\delta)$ the unitary matrix of eigenvectors we have the basic eigenequation $\tilde{H}_D(\delta) X(\delta) = X(\delta)\Lambda(\delta)$.

Next, note that because $\tilde{H}_D(\delta)$ is linear in δ it is differentiable with respect to δ for all δ. With the convention that a prime indicates differentiation with respect to δ, we drop the explicit dependence on δ from the notation and have $\tilde{H}_D' = S_{H_D}$. Differentiating the eigen-equation we have $\tilde{H}_D' X + \tilde{H}_D X' = X'\Lambda + X\Lambda'$ which we can manipulate to $X^{-1}\tilde{H}_D' X - \Lambda' = -X^{-1}\tilde{H}_D X' + X^{-1}X'\Lambda$. This necessitates that X has an inverse, or equivalently that the eigenvalues are pairwise distinct, which holds generically. Indeed, if two eigenvalues cross for some δ, this situation can be removed by an arbitrarily small perturbation of δ.

In keeping with [20] we now define the relation $X' = XC$ so that the last equation above becomes $X^{-1}\tilde{H}_D' X - \Lambda' = -\Lambda C + CA$. Now, we assume that $\overline{X}$ is the matrix of eigenvectors calculated at the nominal point, and we allow for some normalization of the eigenvectors $X = \overline{X}\Gamma$ via a diagonal matrix $\Gamma = \mathrm{diag}\{\gamma_k\}$. Now substituting this into the last equation, we have the final required relation $-\Gamma\Lambda C + \Gamma C\Lambda = \overline{X}^{-1}\tilde{H}_D'\overline{X}\Gamma - \Gamma\Lambda' = \overline{X}^{-1}S_{H_D}\overline{X}\Gamma - \Gamma\Lambda'$. From here we examine this last equation element by element to determine the values of C and thus take $X' = XC$.

For the off-diagonal elements of C, we then have $c_{kl} = \frac{\overline{y}_k{}^* S_{H_D} \overline{x}_l \gamma_l}{\gamma_k(\lambda_l - \lambda_k)}$, where $\overline{x}_k$ is the kth right eigenvector of $H_D +$

S_{H_D} and $\overline{y}_k$ its left eigenvector, $*$ denotes the conjugate transpose, and the λ_k's are the eigenvalues of $H_D + S_{H_D}$. The set $\{\gamma_k\}$, the entries of the matrix Γ, can be taken arbitrarily since multiplying an eigenvector by a constant still returns an eigenvector; however, we stick with the normalization algorithm used in [20]. Let $x_{m,k}$ denote the mth element of the kth eigenvector and likewise for $\overline{x}_{m,k}$; then, we choose to make $x_{m,k} = 1$ so that we can determine γ_k as $\frac{1}{\overline{x}_{m,k}}$. To find which element of $\overline{x}_k$ to designate as the mth, we take $\max_{1\le j\le N} |\overline{x}_{j,k}| \left|\overline{y}_{j,k}\right| = |\overline{x}_{m,k}| \left|\overline{y}_{m,k}\right|$ for each left-right eigenvector pair k. With this, then we can easily determine the off-diagonal elements of C as indicated above, and we use the formula provided in [20] for the diagonal elements of $c_{kk} = -\sum_{\ell\neq k} \overline{x}_{m,\ell}\gamma_\ell c_{\ell k}$ where $\ell = 1,\dots,N$ and $\ell \neq k$. We then finally have the matrix of eigenvalue derivatives as $X' = XC = \overline{X}\Gamma\mathrm{C}$.

C. Structure of fictitious feedback Δ_p

Consider the system initially in a pure state $\rho(0) = |\mathrm{IN}\rangle\langle\mathrm{IN}|$. If $|\mathrm{IN}\rangle$ is perturbed as $U|\mathrm{IN}\rangle$ where U is unitary, then the initial state is perturbed as $\tilde{\rho}(0) = U|\mathrm{IN}\rangle\langle\mathrm{IN}|U^\dagger$. The preparation error is hence $d\rho(0) = \tilde{\rho}(0) - \rho(0)$. Recall that a unitary matrix can be written e^K, with $K = -K^\dagger$. Approximating $U = e^K$ as $U \approx I + K$ yields the first order preparation error

$$d\rho(0) = (I+K)\rho(0)(I+K)^\dagger - \rho(0) = [K, \rho(0)].$$

The preparation error in terms of the Bloch vector $d\boldsymbol{r}(0)$ reads

$$dr_k(0) = \mathrm{Tr}([K,\rho(0)]\sigma_k), \quad k = 1,...,N^2.$$

Since the perturbation w should reproduce the initial state preparation error, it should be structured as

$$w = \begin{pmatrix} \mathrm{Tr}([K,\rho(0)]\sigma_1) \\ \mathrm{Tr}([K,\rho(0)]\sigma_2) \\ \vdots \\ \mathrm{Tr}([K,\rho(0)]\sigma_{N^2}) \end{pmatrix}.$$

By the bottom fictitious loop of Fig. 1, the perturbation w is generated by dz. Hence dz must enter in the above vector. Since $\rho(0)$ is fixed by the selectivity of the controller, the only place where z could enter is through K. Hence K depends on dz, and the linearity of the bottom fictitious loop requires K to be linear in dz; write it $K\{dz\}$. The bottom fictitious loop, $w = \Delta_p dz$, hence defines Δ_p such that

$$\Delta_p z = \begin{pmatrix} \mathrm{Tr}([K\{dz\},\rho(0)]\sigma_1) \\ \mathrm{Tr}([K\{dz\},\rho(0)]\sigma_2) \\ \vdots \\ \mathrm{Tr}([K\{dz\},\rho(0)]\sigma_{N^2}) \end{pmatrix}. \tag{40}$$

holds for all dz's.

The key question is whether, for a given $\rho(0)$, the above equality imposes some structure on Δ_p. By an example, we show that it does.

1) Example: We consider the very simple example of a 2-spin system subject to Lindblad-like decoherence, where the objective is to flip the excitation between the 2 spins: $|1\rangle \to |2\rangle$. Assuming the system is to be controlled to the pure state $|\mathrm{OUT}\rangle\langle\mathrm{OUT}|$, the target state in the state space format is

$$r_{\mathrm{OUT}} = \mathrm{Tr}\left(|\mathrm{OUT}\rangle\langle\mathrm{OUT}| \begin{pmatrix} \frac{1}{\sqrt{2}} I_{2\times 2} \\ x_{12} \\ y_{12} \\ z_1 \end{pmatrix}\right).$$

where x_{12}, y_{12}, and z_1 are elements of the Gell-Mann basis of Sec. III. Specifically,

$$x_{12} = \frac{1}{\sqrt{2}}\begin{pmatrix} 0 & 1 \\ 1 & 0 \end{pmatrix}, \quad y_{12} = \frac{1}{\sqrt{2}}\begin{pmatrix} 0 & -\jmath \\ \jmath & 0 \end{pmatrix},$$
$$z_1 = \frac{1}{\sqrt{2}}\begin{pmatrix} 1 & 0 \\ 0 & -1 \end{pmatrix}.$$

The error dz could be defined as $Cdr(t)$ where C is defined as in Sec. IV.

We start from the right-hand side of the key equation (40) and proceed to write it in the left-hand side format to reveal the structure of Δ_p. We take

$$\rho_0 = \begin{pmatrix} 1 & 0 \\ 0 & 0 \end{pmatrix}$$

and parameterize $K = -K^\dagger$ as:

$$K = \begin{pmatrix} \jmath b_{11}\{dz\} & a_{12}\{z\} + \jmath b_{12}\{dz\} \\ -a_{12}\{dz\} + \jmath b_1 2\{dz\} & \jmath b_{22}\{dz\} \end{pmatrix},$$

where

$$a_{k\ell}, b_{k\ell} \in \mathbb{R}.$$

Because of the linearity of $a_{k\ell}\{dz\}$, $b_{k\ell}\{dz\}$, we write them as

$$a_{k\ell}\{dz\} = A_{k\ell}dz, \quad b_{k\ell}\{dz\} = B_{k\ell}dz,$$

where $A_{k\ell}$, $B_{k\ell}$ are real matrices (and dz is a column vector).

With these conventions, the right hand side of (40) becomes

$$\underbrace{\begin{pmatrix} 0 \\ -\sqrt{2}A_{12} \\ -\sqrt{2}B_{12} \\ 0 \end{pmatrix}}_{\Delta_p} dz. \tag{41}$$

The above reveals the fictitious feedback Δ_p. Call $\mathcal{D}_p$ this structure. Even though A_{12} and B_{12} are arbitrary real matrices, Δ_p is structured from two viewpoints: it is real and the first and last block rows are vanishing. This is contrary to the coherent case where Δ_p is fully populated and complex.

2) Justification for the choice of generalized error: In Sec. IV, a natural choice for the generalized error was a scalar $z(t)$ representing a $\|\cdot\|_1$ norm. We however elected to choose a vector form for $z(t)$ representing a $\|\cdot\|_2$ norm. The reason for this choice can be seen from (41). Indeed, if dz were scalar, $\Delta_p dz$ would not be able to generate the various w's that span a N^2-dimensional space.

TABLE II: Summary of results for the relationship between metrics of interest for the case of uncertainty in the coupling between neighboring spins

Coupling uncertainty summary									
Ring size	Transfer	Probability and μ				Probability and log-sensitivity			
		mean τ	mean Z	mean p	Stouffer p	mean τ	mean Z	mean p	Stouffer p
3	1→1	1.0000	67.0234	0.0000	0.0000	1.0000	67.0234	0.0000	0.0000
3	1→2	-0.0421	-2.8239	0.3396	1.0000	-0.2104	-14.0995	1.0000	1.0000
4	1→1	0.7070	47.3822	0.0000	0.0000	0.9137	61.2393	0.0000	0.0000
4	1→2	0.5377	36.0368	0.0000	0.0000	0.3868	25.9246	0.0000	0.0000
5	1→1	0.4098	27.4648	0.0000	0.0000	1.0000	67.0234	0.0000	0.0000
5	1→2	0.5530	37.0639	0.0000	0.0000	0.6241	41.8266	0.0000	0.0000
5	1→3	0.5364	35.9513	0.0000	0.0000	0.6088	40.8012	0.0000	0.0000
6	1→1	0.6839	45.8362	0.0000	0.0000	0.8941	59.9223	0.0000	0.0000
6	1→2	-0.0910	-6.1014	0.6667	1.0000	0.7176	48.0960	0.0000	0.0000
6	1→3	0.4057	27.1892	0.0000	0.0000	0.4983	33.3978	0.0000	0.0000

TABLE III: Summary of results for the Hypothesis Test applied to cases of bias spillage

Bias spillage summary									
Ring size	Transfer	Probability and μ				Probability and log-sensitivity			
		mean τ	mean Z	mean p	Stouffer p	mean τ	mean Z	mean p	Stouffer p
3	1→1	0.0331	2.2162	0.6667	0.0001	1.0000	67.0234	0.0000	0.0000
3	1→2	-0.0083	-0.5589	0.7119	0.9959	-0.2829	-18.9587	1.0000	1.0000
4	1→1	0.1078	7.2234	0.5000	0.0000	0.9232	61.8743	0.0000	0.0000
4	1→2	0.0242	1.6203	0.1121	0.0006	-0.4076	-27.3204	1.0000	1.0000
5	1→1	0.0054	0.3592	0.8000	0.2109	0.9999	67.0153	0.0000	0.0000
5	1→2	-0.3847	-25.7852	0.8000	1.0000	-0.0034	-0.2279	0.2031	0.6948
5	1→3	-0.2734	-18.3269	0.8000	1.0000	0.0523	3.5040	0.0011	0.0000
6	1→1	0.2420	16.2174	0.1690	0.0000	0.8852	59.3302	0.0000	0.0000
6	1→2	-0.5630	-37.7342	1.0000	1.0000	0.3955	26.5089	0.0000	0.0000
6	1→3	-0.1245	-8.3455	0.6667	1.0000	0.0032	0.2111	0.4789	0.3025

TABLE IV: Summary of the correlation between μ and log-sensitivity

μ and log-sensitivity correlation summary									
Ring size	Transfer	Coupling uncertainty				Bias spillage			
		mean τ	mean Z	mean p	Stouffer p	mean τ	mean Z	mean p	Stouffer p
3	1→1	1.0000	67.0234	0.0000	0.0000	0.0331	2.2162	0.6667	0.0001
3	1→2	0.7378	49.4499	0.0000	0.0000	-0.0370	-2.4821	0.6855	1.0000
4	1→1	0.6871	46.0484	0.0000	0.0000	0.1041	6.9755	0.5000	0.0000
4	1→2	0.1235	8.2740	0.0000	0.0000	0.1041	6.9755	0.5000	0.0000
5	1→1	0.4098	27.4648	0.0000	0.0000	0.0054	0.3592	0.8000	0.2109
5	1→2	0.7838	52.5303	0.0000	0.0000	0.1385	9.2841	0.0062	0.0000
5	1→3	0.7633	51.1603	0.0000	0.0000	0.0928	6.2171	0.0081	0.0000
6	1→1	0.6986	46.8248	0.0000	0.0000	0.2233	14.9663	0.2527	0.0000
6	1→2	0.0708	4.7430	0.6667	0.0000	-0.2950	-19.7685	1.0000	1.0000
6	1→3	0.3879	26.0006	0.0000	0.0000	-0.0806	-5.4021	0.8271	1.0000